

Prolonged energy harvesting for ingestible devices

Phillip Nadeau¹, Dina El-Damak¹, Dean Glettig², Yong Lin Kong², Stacy Mo², Cody Cleveland^{2,3}, Lucas Booth², Niclas Roxhed^{2,4}, Robert Langer^{2,5,6*}, Anantha P. Chandrakasan^{1*} and Giovanni Traverso^{2,3*}

Ingestible electronics have revolutionized the standard of care for a variety of health conditions. Extending the capacity and safety of these devices, and reducing the costs of powering them, could enable broad deployment of prolonged-monitoring systems for patients. Although previous biocompatible power-harvesting systems for *in vivo* use have demonstrated short (minute-long) bursts of power from the stomach, little is known about the potential for powering electronics in the longer term and throughout the gastrointestinal tract. Here, we report the design and operation of an energy-harvesting galvanic cell for continuous *in vivo* temperature sensing and wireless communication. The device delivered an average power of $0.23 \mu\text{W mm}^{-2}$ of electrode area for an average of 6.1 days of temperature measurements in the gastrointestinal tract of pigs. This power-harvesting cell could provide power to the next generation of ingestible electronic devices for prolonged periods of time inside the gastrointestinal tract.

Thanks to recent advances in ingestible electronics, it is now possible to perform video capture¹, electronically controlled drug release², pH, temperature and pressure recording³, and heart rate and respiration monitoring⁴ from within electronic pill-like capsules placed in the gastrointestinal (GI) tract. Recent progress in energy harvesting and wireless power transfer is offering new options to power these devices, but many are not well suited to ingestible capsules. For example, traditional harvesting sources such as thermal⁵ and vibration⁶ energy harvesting are complicated by the lack of thermal gradients in the stomach and challenges in obtaining mechanical coupling to motion sources. Wireless power-transfer via near-field⁷ or mid-field⁸ coupling is also challenging in this case, due to the unconstrained position and orientation of the capsule. Hence, most current ingestible electronics still rely on primary cell batteries, many of which require toxic materials, have limited shelf life due to self-discharge and can cause mucosal injury⁹. There is therefore a need to explore alternative sources, particularly as the circuits scale to lower average power.

A few key trends have led to our work. For one, the average power demands of complementary metal-oxide-semiconductor (CMOS) technology have been decreasing, now reaching the nanowatt level thanks to advanced design techniques and technology improvements^{10–12}, enabling a wider array of harvesters. Next, advances in material design and packaging have demonstrated fully passive gastric devices that are small enough to be swallowed, but then unfold after ingestion to remain up to seven days in the stomach for long-term drug delivery¹³. Such devices could one day provide an ingestible non-invasive platform for active wireless electronic sensors that perform long-term *in vivo* vital signs monitoring. Finally, interest in biocompatible galvanic cells is rising, with a focus on (1) transient electronics that fully disappear at the end of their tasks¹⁴, (2) electrolytes that are supplied on demand to extend the shelf life of the cell¹⁵,

(3) material selection for fully biocompatible and biodegradable cells^{14–17} and recently, (4) edible gastric Mg–Cu cells, which can power near-field communication of medication compliance information to a body-worn patch for up to a few minutes¹⁸. Additional support for the potential of long-term harvesting is provided by two *in vitro* studies on cells in synthetic gastric-fluid-like electrolytes, which demonstrated measurements lasting a number of hours^{19,20}.

This has led us to investigate the practical use of a biocompatible galvanic cell for powering a wireless sensor node in the GI tract. Here, we report an energy-harvesting system with temperature sensing and wireless communication, evaluated in a porcine model. We demonstrate a fully autonomous sensor system, created from commercial semiconductor parts, and powered solely by the cell and capable of providing central temperature measurements. The device can also use the harvested power to activate drug release via electrochemical dissolution of a gold membrane.

Results

Basic principle and initial characterization. The bio-galvanic cell characterized in this work consists of a redox couple formed by a dissolving metallic anode that undergoes galvanic oxidation and an inert cathode that returns electrons to the solution. In our case, the gastric or intestinal fluids of the surrounding environment form the electrolyte. The final performance of the cell is a strong function of the environmental conditions that change significantly during normal gastrointestinal routines. For example, the pH, chemical composition and heterogeneity of the stomach contents²¹ vary considerably throughout the day. Hence the performance of the cell needs to be ascertained directly by *in vivo* characterization. As previous studies have noted^{14,22}, the cathodic reaction proceeds with either hydrogen gas evolution or by the reduction of dissolved oxygen gas, depending on the pH of the solution,

¹Department of Electrical Engineering and Computer Science, and the Microsystems Technology Laboratories, Massachusetts Institute of Technology, Cambridge, Massachusetts 02139, USA. ²Department of Chemical Engineering and Koch Institute for Integrative Cancer Research, Massachusetts Institute of Technology, Cambridge, Massachusetts 02139, USA. ³Division of Gastroenterology, Brigham and Women's Hospital, Harvard Medical School, Boston, Massachusetts 02115, USA. ⁴Department of Micro and Nanosystems, KTH Royal Institute of Technology, 10044 Stockholm, Sweden. ⁵Media Lab, Massachusetts Institute of Technology, Cambridge, Massachusetts 02139, USA. ⁶Institute for Medical Engineering and Science, Massachusetts Institute of Technology, Cambridge, Massachusetts 02139, USA. *e-mail: ctraverso@partners.org; rlanger@mit.edu; anantha@mtl.mit.edu

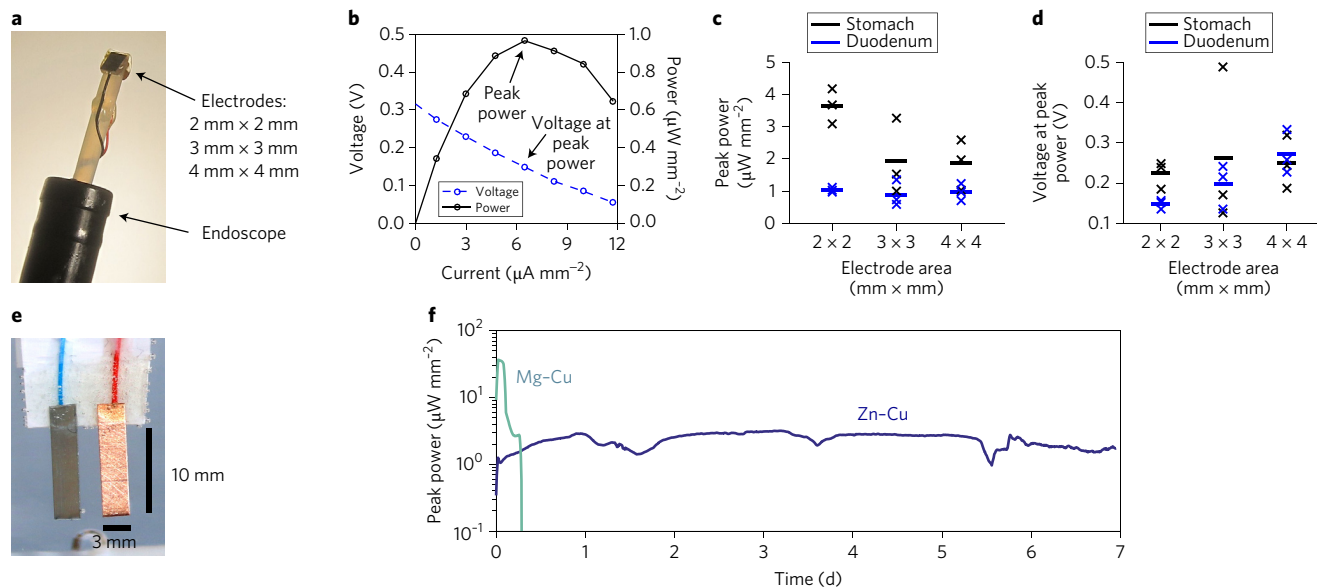


Figure 1 | Initial *in vivo* characterization and anode comparison. **a**, Mg-Cu electrodes for probing the available power *in vivo* in different areas of the stomach and duodenum, with results shown in **b-d**. **b**, Example of measured electrode voltage and output power density versus load current density (2 × 2 mm electrodes; duodenum). **c**, Measured peak power density (horizontal bars denote mean), taken at the peak indicated in **b**, for different electrode sizes and locations ($N=3$). **d**, Voltage at peak power in **c** ($N=3$). **e**, Electrode configuration for anode comparison *in vitro* with measurements given in **f**. **f**, Measured peak power density over time for both anode configurations. Average peak-power was $13.0 \mu\text{W mm}^{-2}$ for the Mg anode (lifetime, 0.3 days) and $2.3 \mu\text{W mm}^{-2}$ for the Zn anode (lifetime, >7.0 days).

and is usually limited by mass-transport conditions. The relevant cathodic reactions are given by:



A number of materials have been proposed as dissolving anodes, most prominently, magnesium^{18,23} and zinc^{15,19,20}, which are noted for their dietary value²⁴, manufacturability, low cost and relatively low position in the electrochemical series²⁵. The reaction at the anode is given by:



where $X = \text{Mg}$ or Zn . The cathode, which sends electrons back into the solution, was created from pure copper metal²⁶.

Given prior successes in utilizing magnesium, which has a higher reduction potential, for *in vivo* power generation¹⁸, we first considered magnesium anodes for our initial *in vivo* characterization evaluating the impact of electrode size. In Fig. 1a–d, we characterized a Mg–Cu electrode system in a porcine model using small square electrodes of differing areas, mounted on the tip of an endoscope as shown in Fig. 1a (see Methods). The current density was stepped in fixed increments resulting in the voltage and power densities shown in Fig. 1b. The resulting average peak power density across all sizes shown in Fig. 1c was $2.48 \mu\text{W mm}^{-2}$ in the stomach ($0.97 \mu\text{W mm}^{-2}$ in the duodenum), and the average observed cell voltage in Fig. 1d was 0.23 V. Consistent with the low observed cell voltage, we also noted a large amount of corrosion on the magnesium electrodes, suggesting that the lifetime of a magnesium-based prototype would not exceed 24 h, thereby making week-long wireless measurements unfeasible.

Motivated by the observations of corrosion and given the intention to evaluate extended gastric residence of these electrodes, we performed extended *in vitro* studies of electrode longevity (see Methods). With the configuration shown in Fig. 1e,

we compared Mg and Zn anodes in side-by-side measurements using a load-sweep methodology (50 k Ω down to 150 Ω in 255 steps). Figure 1f shows the maximum power observed in each load resistance sweep. For the Mg anode, the cell voltage was 1.3 times higher and the peak power density was 6 times higher, but the Zn anode lasted much (>23 times) longer, suggesting that Zn was the better choice for longer-term use. The combination of the experiments presented in Fig. 1 allowed us to proceed to the design of a zinc-based measurement capsule to enable evaluation of the power parameters via a stand-alone device *in vivo*.

Characterization in the stomach environment. We created a measurement capsule (Fig. 2 and Methods) to obtain detailed measurements of the performance of the Zn–Cu cell in a porcine stomach and transmit the results to a nearby base station. The design was fully self-sufficient and wireless to avoid a tether to the outside that could reduce the practical measurement duration or impact the comfort or normal routines of the animal. A conventional coin-cell battery powered the capsule to avoid loading the electrodes with the demands of the circuitry during measurement, allowing a precise characterization of the cell with a separate controllable load.

The capsule was created using all commercial low-cost semiconductor parts (Fig. 2a–c) and consisted of an 8 bit digitally controlled potentiometer²⁷ to set the load resistance of the cell, and a microcontroller system on a chip²⁸ and its associated peripherals, which contained (1) a 10 bit analogue-to-digital converter (ADC) that measured the electrode voltage, (2) a temperature sensor, (3) a wireless transmitter and (4) a processor that ran software code to control all of the functions.

To characterize the cell, the software was programmed to sweep the load resistance through all 256 available codes (50 k Ω down to 150 Ω in 255 linear steps), taking voltage measurements at each point. Each step was held for 2 s, and at the end of a sweep, the resistor was reset to 50 k Ω and held for a further 64 s for the electrode voltage to re-equilibrate to the light-load condition before starting the next

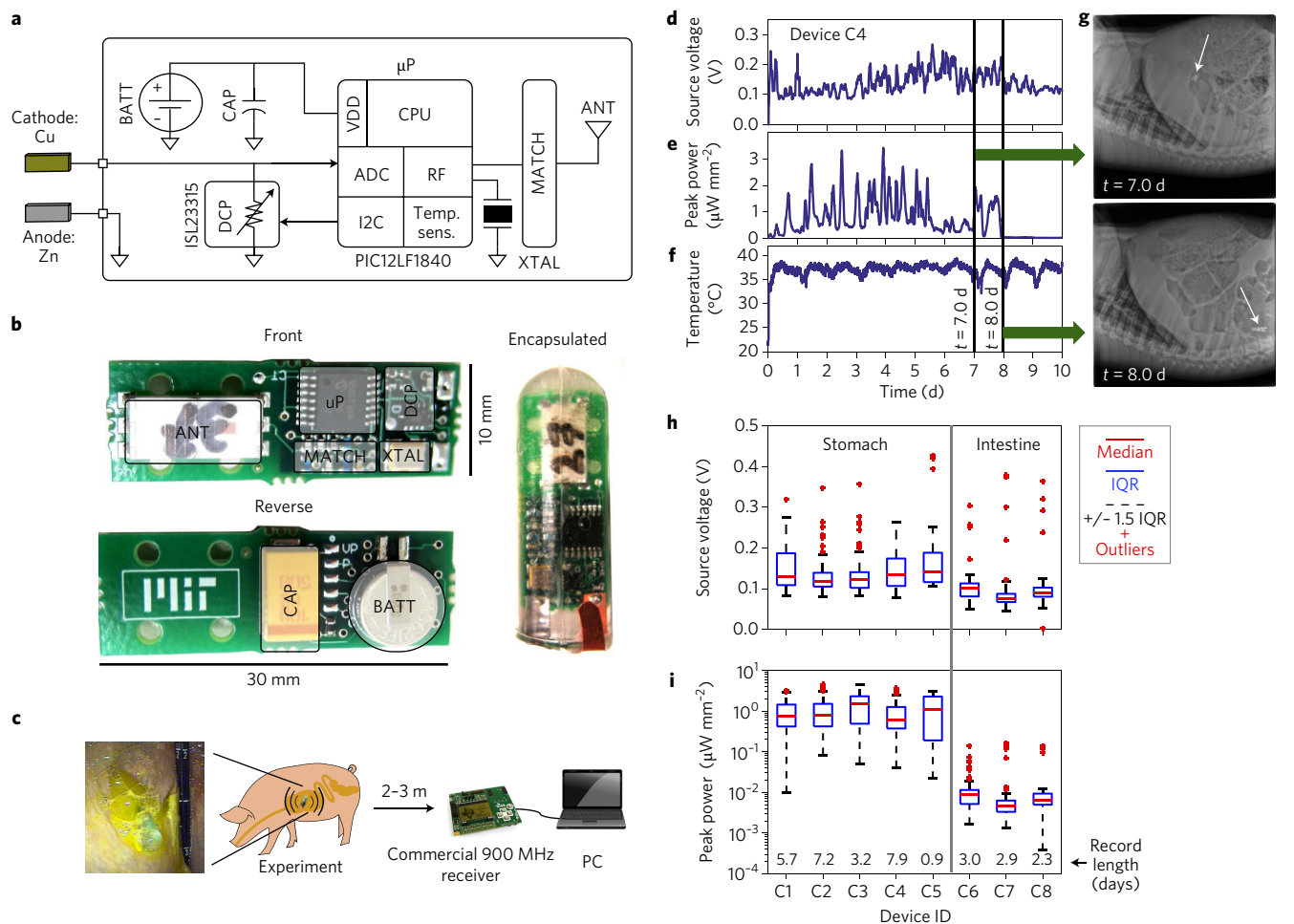


Figure 2 | Electrical characterization of the gastric battery in a porcine model. **a, b**, Schematic of measurement-system architecture (**a**) and photographs of the front and reverse sides of the system along with encapsulation using epoxy and PDMS (**b**). The printed circuit board includes a programmable load resistor (DCP; part no. ISL23315), crystal (XTAL), microcontroller (μP ; part no. PIC12LF1840), radio frequency transmitter (RF), a serial interface (I2C), and a temperature sensor (Temp. sens.). **c**, Diagram of the experimental set-up, including a photograph of the encapsulated pill in contact with gastric fluid inside the porcine stomach. **d-f**, *In vivo* power characterization for a representative device (C4) including the voltage at the point of peak power extraction during each sweep frame (**d**), the peak extracted power in each frame (**e**) and the measured body temperature (**f**). **g**, X-rays at two time points showing passage from the stomach to the small intestine corresponding to the observed drop in power in **e**. **h**, Statistical summary of the source voltage characterization data for eight deployed devices (window size, 1h; IQR, interquartile range). **i**, Corresponding peak power measurements for the eight devices.

measurement (full measurement time: 576 s per sweep). The data, which included electrode voltages at each of the 256 resistor-codes, and the temperature sensor measurements, were transmitted as a frequency-shift-keying-modulated, +10 dBm, 920 MHz wireless signal, to a commercial base-station receiver, mounted about 2 m away—a flow diagram for the resistance-sweep methodology and examples of measured waveforms are shown in Supplementary Figs 1 and 2, respectively. Prior to the animal experiments, we also performed *in vitro* characterization of the Zn–Cu cell and measurement electronics in synthetic gastric fluid (SGF; data shown in Supplementary Fig. 3).

The measurement capsule was initially deployed in five animals with the results summarized in Fig. 2d–i and full data shown in Supplementary Figs 4 and 5 (see Methods for experimental details). Due to the slow motility of the porcine GI tract^{29,30} and the size of the capsule, the devices were retained in the animal for seven to ten days without additional design considerations. During this time, the data were collected as the animal carried out its normal daily routines. The traces in Fig. 2d–f correspond to an example device, and show

the electrode voltage measured at the point of maximum power density for each load resistance sweep (one sample every 576 s), as well as the associated peak power density level, and the temperature recorded by the temperature sensor. Figure 2h,i gives the statistics of the measured peak power and optimum source voltage. Across all five stomach-deployed capsules, the mean time for which power was available, the mean peak power, P_{max} , and the mean voltage at P_{max} were 5.0 days, $1.14 \mu\text{W mm}^{-2}$ and 0.149 V, respectively. There was a large amount of variation in the transit time of the devices, which was anticipated and consistent with previous observations of the porcine GI tract^{29–31}.

Interestingly, by correlating the anatomic location of the capsule determined through serial X-rays, we demonstrated that the peak power drops significantly after passage through the pylorus to the small intestine. The combination of Fig. 2e,g shows an example of this correlation. To confirm this observation, we deployed three devices directly into the small intestine and tracked their passage through the colon until exit. The three devices showed an average of 13.2 nW mm^{-2} of peak power density and the power remained

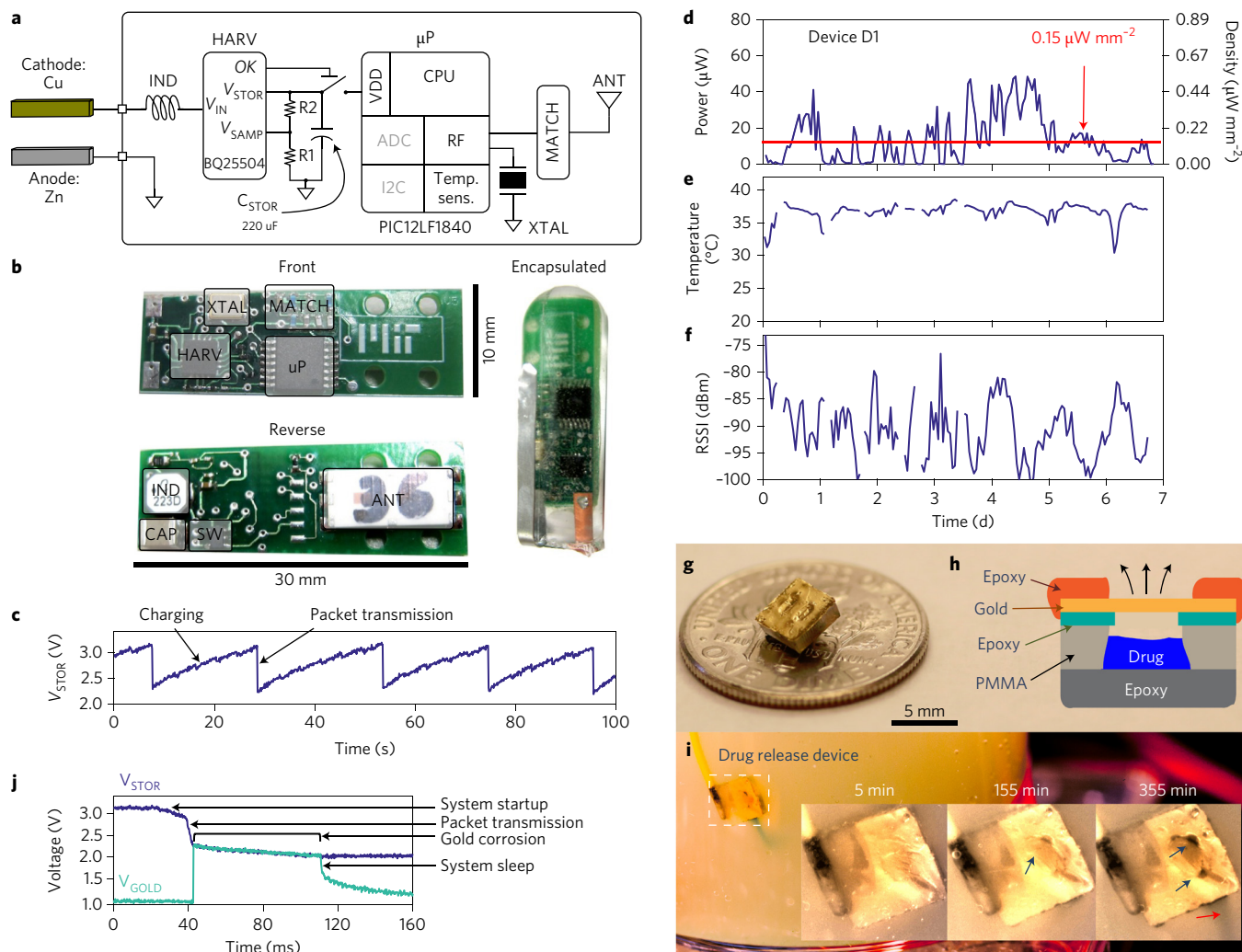


Figure 3 | Demonstration of galvanic-cell-powered gastric temperature measurement, wireless transmission and drug delivery. **a**, Architecture of the harvesting system. **b**, The fabricated and encapsulated system printed circuit board. **c**, Snapshot of storage capacitor during continuous harvesting in SGF. **d**, Example of the full *in vivo* measurement data for a representative device (D1), including the estimated average power harvested by the board in one-hour windows versus time, and the overall average power (red line). **e**, *In vivo* measurement of the body temperature performed using the harvested power. **f**, Received signal strength indication (RSSI) at the receiver for packets transmitted from the body using the harvested power. In **e**, **f**, discontinuities indicate times for which power was unavailable to send packets. **g**, Photo showing scale of drug release prototype device versus a United States dime. **h**, Cross-sectional view of the device in **g**, where methylene blue is contained in a PMMA reservoir sealed with a 300 nm gold membrane and epoxy. **i**, Self-powered release (blue outflow) from bottom right of the device (gold block; dashed white box indicates area magnified in inset) after activation in a beaker of porcine gastric fluid. Inset shows sequential images where the simulated drug (blue dye) is released via corrosion of the gold membrane. The membrane is intact in the beginning ($t = 5$ min) before triggered corrosion weakens it, causing cracks to form after 155 min (as shown by blue arrows), and ultimately the release of significant amounts of blue dye as shown at 355 min (indicated by the red arrow). **j**, Electrical profile during delivery of a charge pulse to the release electrode; V_{STOR} , storage capacitor voltage; V_{GOLD} , voltage on the gold release electrode.

present, between 1 and 100 nW mm⁻², throughout the passage time until exit (Supplementary Fig. 4).

Harnessing power *in vivo* for sensing, communication and drug delivery. To demonstrate the utility of the energy obtained, we created a second capsule powered entirely by the Zn–Cu cell (Fig. 3 and Methods). This harvested power was used for all functions of the capsule, which included temperature measurement, software control and wireless transmission to a base station located 2 m away. In this design (Fig. 3a), we used a commercial energy-harvesting boost-converter integrated circuit³², which took energy directly from the Zn–Cu cell at low voltage (0.1–0.2 V) and boosted it onto a temporary storage capacitor at a higher voltage (2.2–3.3 V) for use by the circuits. The encapsulated sensor device prepared for deployment is shown in Fig. 3b.

When the input source is applied, the boost converter integrated circuit pulls energy from the input voltage (V_{IN}) and transitions through a start-up region. Once the start-up is complete, the main higher-efficiency boost converter is activated and sets the OK signal, which then powers the microcontroller through a switch. From here, the microcontroller transmits packets containing temperature measurement data at a variable rate depending on the input power. Figure 3c shows an example of steady-state operation of the capsule, where the storage capacitor is slowly charged until enough energy is available for packet transmission. The system regulates the rate by periodically sampling the supply voltage, V_{DD} , to determine whether to send a packet or wait for more energy to be harvested. If the sampled voltage is below 3.0 V, the system remains in a low-energy sleep mode for 4 s before

attempting to sample again. If the voltage is above 3.0 V, the system transmits a packet and then returns to periodically sampling the voltage (initially 0.5 s after the packet, and then again every 4 s) to determine when to transmit the next packet. Further details on the capsule design and operation are provided in Supplementary Figs 6–8.

Since packet transmission is the dominant energy consumer, we used the number of transmitted packets in a given window of time (t_{window}) to estimate the overall amount of energy delivered to the load. Each packet is 176 bits long including preamble and headers and is transmitted at 50 kbps, resulting in a 3.5 ms packet transmitted at +10 dBm. Prior to the experiments, a laboratory source-meter was used to characterize the energy consumed by the capsule in transmitting each packet as a function of the V_{DD} for the system: $E_{\text{pkt}} = f(V_{\text{DD}})$. Then during the *in vivo* experiment, the number of packets transmitted during a given interval was used to determine the average power ($P_{\text{sys,ave}}$) delivered to the load using:

$$P_{\text{sys,ave}} = \frac{1}{t_{\text{window}}} \sum_{\text{all } m} E_{\text{pkt}}(V_{\text{DD}}(m)) \quad (4)$$

where m represents a packet and Σ is the sum over all the packets transmitted within t_{window} . $V_{\text{DD}}(m)$ is the measured system V_{DD} at the beginning of each packet transmission—information that was transmitted along with the temperature measurement data. To obtain an accurate packet count despite the possibility of dropped packets, we also transmit an internally generated packet count to the base station along with the other measurements.

The system was deployed in three animals and the results are summarized in Table 1 (full measurements in Supplementary Fig. 9). Figure 3d shows the power delivered from the cell to the load using equation (3), with $t_{\text{window}} = 1$ h. Figure 3e shows the measured temperature sensor data, and Fig. 3f shows the radio frequency signal strength seen by the receiving base station for each packet. Of note was that temperature readings below the expected core or central temperature were observed to coincide with daytime hours and times around feeding (Fig. 3e), probably representing transient temperature decreases associated with ingestion of foods and liquids. The disconnected regions in the figures represent periods for which electrical power was not sufficient to send wireless packets; for example, due to variations in both the fluidic environment of the stomach and the position of the capsule within it. On average, packets were received in 91% of the 1 h time slots during the three experiments. Across all of the experiments, the devices operated for a mean of 6.1 days, delivering an average power of $0.23 \mu\text{W mm}^{-2}$ to the load, and transmitting packets with temperature measurements every 12 s.

To further demonstrate the utility of the energy harvested by the system, we designed and fabricated a device for drug release that can be triggered with the harvested energy, as shown in Fig. 3g, and tested this device *in vitro* with physiologic gastric fluid (see Methods for the details of device fabrication). The device, as shown in Fig. 3h, encapsulates a model drug (in this case, methylene blue) in a poly(methyl methacrylate) (PMMA) reservoir ($2.0 \times 1.0 \times 1.5$ mm) that is sealed with a 300-nm-thick gold membrane. The release is achieved via electrochemical dissolution of the membrane, as demonstrated previously by Santini *et al.*³³. The gold membrane, which is otherwise inert in the gastric environment, can be chemically corroded when the potential is raised (+1.04 V with respect to a saturated calomel reference electrode) to allow formation of water-soluble chloro-gold complexes³⁴. Our results show that the device remains intact when it is connected to the system ground (shorted to the zinc electrode) in physiologic gastric fluid (see Methods for experimental details). On activation via the application of discharge from 2.0 to 2.3 V with respect to the zinc system ground, the

Table 1 | Summary of the *in vivo* performance of three ingestible devices in a porcine model.

Device	Time (d)	Average packet interval (s)	Average power delivered (μW)	Average power density ($\mu\text{W mm}^{-2}$)	Total energy density (mJ mm^{-3})
D1	6.82	15.7	13.6	0.151	177
D2	6.61	14.0	16.0	0.178	203
D3	4.73	6.8	32.0	0.356	292

For power and energy density, the electrode area ($30 \text{ mm} \times 3.0 \text{ mm}$) was used. For energy density, the combined thickness of the two electrodes ($500 \mu\text{m}$ total) was used.

corrosion of the gold weakens the membrane integrity, causing cracks that are visible at $t = 155$ min in Fig. 3i (blue arrow in middle inset), and ultimately visible release of the contents (red arrow in right inset of Fig. 3i) through the corroded membrane. The voltage profile plotted in Fig. 3j shows the discharge characteristics that gradually activate the release. The initial shallow ramp from 3.15 to 2.95 V represents the microcontroller boot-up followed by temperature measurement. The steep drop from 2.95 to 2.30 V represents the packet transmission, and the slower discharge from 2.30 to 2.00 V represents charges delivered to the gold electrode. With the $220 \mu\text{F}$ storage capacitance, this represents $66 \mu\text{C}$ of charge delivered to the electrode per pulse. The pulse ends when the boost converter toggles the OK signal to low (due to the storage voltage declining below the threshold), which deactivates the microcontroller and release-electrode switch, and allows the storage capacitor to begin charging in preparation for the next cycle. The average pulse interval during the experiment was 11.9 s, and the charge delivery rate was $5.5 \mu\text{C s}^{-1}$. For the designed size of the active gold area ($2 \text{ mm} \times 1 \text{ mm}$; thickness, 300 nm), the total theoretical charge necessary to completely dissolve the electrode was 17.0 mC, and hence an ideal dissolution time of 51 min. In gastric fluid, it is expected that side reactions can occur on the electrode surface resulting in a longer release time, hence the observed time of 155 min.

Discussion

Ingestible electronics have an expanding role in the evaluation of patients³⁵. The potential of applying electronics or electrical signals for treatment is being explored³⁶ and the potential for long-term monitoring and treatment is being realized through the development of systems with the capacity for safe, extended gastrointestinal residence^{13,37}. Energy alternatives for GI systems are needed to enable broad applicability, especially given size and biocompatibility constraints coupled with the need for long-term power sources and low-cost systems.

Here, we report the *in vivo* characterization of a galvanic cell composed of inexpensive biocompatible materials, which are activated by GI fluid. We demonstrated energy harvesting from the cell for up to six days (average power, $0.23 \mu\text{W mm}^{-2}$) and using this energy we developed a self-powered device with the capacity for central temperature measurement and wireless transmission from within a large animal model. Combining the cell with a boost converter in the energy harvesting integrated circuit allowed the system to power these more complex electronics, even as the cell voltage and power varied during experiments.

The device we have fabricated could be rapidly implemented for the evaluation of core body temperature and for the evaluation of GI transit time given the differential temperature between the body and the external environment. A recent study evaluating data collected from 8,682 patients found that peripheral temperature readings did not have acceptable clinical accuracy to guide clinical decisions³⁸. Hence, continuous automated central temperature measurements via a wireless ingestible system may provide significant clinical benefit. We also demonstrated, via a custom-designed

drug-release device, that such an energy-harvesting method could be used to activate drug delivery via corrosion of a gold membrane. This proof of concept could ultimately allow the incorporation of drug delivery into the ingestible electronic capsule.

Furthermore, we characterized and demonstrated the capacity to harvest energy from across the GI tract, including the stomach, small intestine and colon. Interestingly, the available power density ranged between a few $\mu\text{W mm}^{-2}$ down to a few nW mm^{-2} across the GI tract. The reduced power in the intestine could potentially be explained by anatomical differences between it and the stomach—for example, diffusion could be impaired by close contact with the intestinal walls. Further development will be required to elucidate the exact causes and could lead to an improved design. In the meantime, these observations may guide future development of gastrointestinal resident electronic power-harvesting systems according to their targeted anatomic location. For example, there may be a need for greater storage capability to carry energy from the stomach, or depending on the application, it may be necessary to support even-lower power modes.

Our electrode area was limited by the availability of a nanowatt-level commercial harvester. Nevertheless, the total elemental zinc present in the largest electrode we tested ($30\text{ mm} \times 3.0\text{ mm} \times 0.25\text{ mm}$) was 161 mg. Assuming the extreme case of full dissolution across the six-day experiment, the average zinc ion deposition rate for this electrode would be 27 mg d^{-1} . This amount is below the US Food and Nutrition Board recommended upper limit of 40 mg d^{-1} (ref. 24), and in line with levels found in over-the-counter zinc supplements (15, 30 and 50 mg d^{-1} doses are commonly available). Looking ahead, we would expect that a custom designed system would be able to target much lower power levels and hence integrate smaller electrodes and incur less zinc deposition.

Research in ultralow-power electronics continues to push the boundaries in terms of average power consumption, and it has already provided a range of options for circuits that could be adapted for use in GI applications at the nanowatt level. Examples include energy harvesters (for $<10\text{ nW}$ of available power^{10–12}), ADCs and signal acquisition circuits ($<10\text{ nW}$ ^{39,40}), far-field wireless transmitters ($<1\text{ nW}$ standby⁴¹), and millimetre-scale sensor nodes with sensing and processing ($<\text{nW}$ standby⁴²). Such systems could allow the electrode dimensions to scale to just a millimetre or two in width and length, and could enable broad applications for extended power harvesting from alternative cells for long-term monitoring of vital signs⁴ and other parameters in the GI tract, especially with the introduction of devices that are deployed endoscopically⁴³ or self-administered¹³ and have the capacity to reside in the gastric cavity for prolonged periods of time.

Though sufficient for our animal studies, one limitation is the size of the capsule. Without a clear picture of the expected voltage and *in vivo* power levels at the outset, achieving further miniaturization as part of this study would have been difficult. Given our measured results, and with further development of the fabrication process—for example, production of a custom single-chip application-specific integrated circuit using improved packaging techniques like component stacking—the design could potentially be reduced to between one-third and one-fifth of its present volume. In addition, future work should strive to match animal behaviour information, such as feeding and motion data, with the measured power level and observed physiological signals to better understand the sources of variation observed here.

One further limitation is the physical design of the electrochemical cell. Our focus was on powering robust *in vivo* measurements over longer periods of time compared with previously reported galvanic cells. However, future work should include efforts to improve the voltage and power of the cell; for example, by integrating membranes to improve proton exchange²⁰ while controlling corrosion of the electrodes⁴⁴. In addition, improving the efficiency of low-voltage

boost converters at ultralow power levels will facilitate use of smaller electrode areas (approaching $1\text{ mm} \times 1\text{ mm}$), or allow energy harvesting across the entire GI tract. Another important direction of future research will be the development of systems that can be safely retained in the GI tract over long periods, thereby enabling self-powered monitoring on the order of weeks, months or even years following a single ingestion. This work should focus on solving material-, packaging- and interface-related challenges in order to design a capsule for eventual human trials.

Methods

Magnesium, zinc and copper electrode fabrication and attachment.

All electrodes were created from pure metal foils (Alfa Aesar, 0.25 mm thick) and cut to the specified dimensions to within $\pm 10\%$. Attachment of the zinc and copper electrodes to wires or to the printed circuit boards (PCBs) was performed with standard solder and flux, whereas magnesium, which is not solderable, was attached via two-part silver conductive epoxy (8331, MG Chemicals).

***In vivo* characterization of Mg–Cu system.** Electrodes (with attached wires) were fixed via thermoplastic adhesive to opposite sides of a 3D-printed post (length, 30 mm; diameter, 3.8 mm) for easy mounting on an endoscope for guidance into the stomach and duodenum. The electrodes were connected by an $\sim 3\text{ m}$ long cable that passed through the lumen of the endoscope to a Keithley 6430 source-meter, which executed the specified current steps and voltage measurements from outside the animal.

Electrode longevity comparison. Electrode anode and cathode (with attached wires) were placed side-by-side (3 mm separation) on a polystyrene support and fixed using 2-part epoxy (20845, Devcon), with 10 mm electrode length exposed. The electrode pairs were submerged in a pH 4 buffer solution (33643, Fluka Analytical) and measured using the same electronics as the capsule; described below.

Capsule fabrication. The PCBs for the capsules were four-layer FR4, with $35\text{-}\mu\text{m}$ copper metallization. The electrodes were soldered onto the PCB for protrusion outside the encapsulation. Encapsulation was performed as a two-step process. Prior to polydimethylsiloxane (PDMS) moulding, the boards were fully coated in two-part epoxy (1–2 mm thick) to act as sealant against moisture and prevent fluid from entering the device via the protruding electrodes. The outer layer was PDMS (Sylgard 184, Dow Corning), selected for biocompatibility with the stomach environment and moulded into a capsule shape to facilitate passage through the GI tract. The electrodes protruded through the back of the encapsulated device and were bent around towards the front and secured to the outer layer of the PDMS with two-part epoxy (20845, Devcon).

***In vivo* characterization.** All procedures were conducted in accordance with the protocols approved by the Massachusetts Institute of Technology Committee on Animal Care. *In vivo* porcine studies were performed in female Yorkshire pigs aged between four and eight months and weighing approximately 45–50 kg. The porcine model was specifically selected on the basis of previous studies indicating a relatively slow transit time, which allows for extended residence of a macroscopic device in the GI tract^{29,30}. Animal sample size was guided by prior proof-of-concept studies of gastrointestinal drug delivery and sensor systems^{13,45}. The *in vivo* experiments were not blinded or randomized. Prior to endoscopy or administration of the prototypes, the animals were placed on a liquid diet for 48 h and then fasted overnight prior to the procedure. The next day, anaesthesia was induced via intramuscular injections of 5.00 mg kg^{-1} Telazol (tiletamine/zolazepam), 2.00 mg kg^{-1} xylazine and 0.04 mg kg^{-1} atropine. The pigs were then intubated and anaesthesia was maintained using inhaled isoflurane (1–3%). For the deployment of the capsule prototypes, the animals were sedated via intramuscular injection of the above agents. The oesophagus was intubated and an oesophageal overtube was inserted (US Endoscopy). The prototypes were delivered directly to the gastric cavity or endoscopically placed in the small intestine via the overtube. Prototype deposition was followed by a series of X-rays. A total of five stomach-deposited characterization devices were evaluated in five separate pig experiments. One device (C1) was retrieved early from the small intestine after recording for 8.3 d and passing through the pylorus. Two devices stopped their recording early owing to leakages in the PDMS/epoxy encapsulation: one after 7.1 d of measurement but prior to reaching the small intestine (C2), and one after 10.1 d of measurement, including 8.0 d in the stomach and 2.1 d spent in the small intestine (C4), as estimated by the observed power density drop. Two devices (C3 and C5) recorded all the way to exit (8.8 and 7.5 d of recording). The four devices reaching the small intestine exhibited significant power density drops coinciding with extra-gastric location. Three additional characterization devices (C6 to C8) were deployed directly into the duodenum to confirm the power density differential, all of

which recorded from deposition until exit (3.0, 2.9 and 2.3 d, respectively). Finally, three self-powered temperature devices (D1 to D3) were evaluated in three separate pig experiments (6.8, 6.6 and 4.7 d, respectively). All three self-powered devices were deployed in the gastric cavity. Before placing the devices, the electrodes were temporarily supplied with 3 V from an external source to ensure cold-start of the harvester and to obtain a temperature reading from the room for offline calibration of the temperature measurement data. During and after the experiment, we did not see evidence of toxicity from clinical observations. While in place, animals were maintained on a liberalized diet.

Drug-release prototype fabrication. Drug cavities and the substrate of the release prototype were first defined with a conventional carbon dioxide laser engraver (Universal Laser Systems VLS 6.60, Engraving Systems LLC) on a 1.5-mm-thick PMMA board (KJ-35052050, McMasterCarr). A 300-nm-thick gold layer was deposited on a separate PMMA substrate using an electron beam evaporator and a polyvinyl alcohol (PVA) film was adhered to the gold surface. The gold-PVA layer was then peeled off from the substrate and transferred to the delivery device to seal the cavity by stamping the device into a thin layer of low viscosity epoxy (EPO-TEK 301-1, Epoxy Technology). The PVA film acts as a dissolvable temporary support layer to provide mechanical rigidity for the thin (300 nm) gold film during the transfer process. Methylene blue (M9140, Sigma Aldrich) was then added to the reservoir (accessible from the bottom of the device) before it was sealed with high viscosity epoxy (20445, Devcon). The relatively high viscosity prevents infiltration of the sealant into the filled cavity. Following curing of the epoxy, the sealed device was put into deionized water to dissolve the temporary PVA film and subsequently dried in air. An electrical connection was then made to the gold layer using conductive epoxy (CW2400, Circuitworks). Finally, all conductive areas except the membrane portion of the gold layer covering the drug cavity were insulated with medium-viscosity ultraviolet-curable epoxy (EPO-TEK OG116-31, Epoxy Technology) and subsequently cured using ultraviolet light.

Demonstration of activated drug release. The release prototype and zinc and copper electrodes (preparation as described earlier; length, 30 mm; width, 3 mm) were submerged in physiologic gastric fluid. Gastric fluid was endoscopically extracted from live Yorkshire pigs that were on a liquid diet two days prior to the procedure. The drug release prototype was connected to a controller board (as described earlier), which harvests energy and then releases it to the prototype. The demonstration proceeded in two phases, (1) the control phase and (2) the release phase. In the control phase, the integrity of the device was first tested in gastric fluid (47 h), while the potential of the gold membrane was maintained at the system ground voltage (0 V relative to the zinc). On determination of its mechanical integrity, and examining the membrane for leakage, the reservoir along with harvesting electrodes were placed in a fresh sample of gastric fluid for the release phase. In this phase, the controller was configured to short the reservoir electrode to the system storage-capacitor voltage, V_{STOR} , to deliver packets of charge at the end of each wake-up interval so as to corrode the electrode. While submerged in gastric fluid, the device was observed through a macroscopic lens, and the electrical profile was recorded using an oscilloscope.

Data collection. A commercial transceiver evaluation board (SmartRF TrxEB, Texas Instruments) was used to receive the 900 MHz FSK packets transmitted from the capsules. For the large animal experiments, the board and its antenna were mounted above the steel cage area that housed the animals (about 2 m above the ground). The transceiver board was connected via USB cable to a laptop that saved the raw packet information for later offline processing in MATLAB version 2014b (MathWorks).

Code availability. The microcontroller code that was used in this study is available in figshare with the identifier doi:10.6084/m9.figshare.4451420 (ref. 46). Certain proprietary code from Microchip Inc. that was used in the microcontroller is not publicly available.

Data availability. Source data for the figures in this study are available in figshare with the identifier doi:10.6084/m9.figshare.4451420 (ref. 46). The authors declare that all other data supporting the findings of this study are available within the paper and its Supplementary Information.

Received 16 May 2016; accepted 19 December 2016; published 6 February 2017

References

- Iddan, G., Meron, G., Glukhovskiy, A. & Swain, P. Wireless capsule endoscopy. *Nature* **405**, 417 (2000).
- van der Schaar, P. J. *et al.* A novel ingestible electronic drug delivery and monitoring device. *Gastrointest. Endosc.* **78**, 520–528 (2013).
- Maqbool, S., Parkman, H. P. & Friedenberg, F. K. Wireless capsule motility: comparison of the SmartPill(R) GI monitoring system with scintigraphy for measuring whole gut transit. *Dig. Dis. Sci.* **54**, 2167–2174 (2009).
- Traverso, G. *et al.* Physiologic status monitoring via the gastrointestinal tract. *PLoS ONE* **10**, e0141666 (2015).
- Ramadass, Y. K. & Chandrakasan, A. P. A battery-less thermoelectric energy harvesting interface circuit with 35 mV startup voltage. *IEEE J. Solid-State Circuits* **46**, 333–341 (2011).
- Dagdeviren, C. *et al.* Conformal piezoelectric energy harvesting and storage from motions of the heart, lung, and diaphragm. *Proc. Natl Acad. Sci. USA* **111**, 1927–1932 (2014).
- Waters, B. H., Sample, A. P., Bonde, P. & Smith, J. R. Powering a ventricular assist device (VAD) with the free-range resonant electrical energy delivery (FREE-D) system. *Proc. IEEE* **100**, 138–149 (2012).
- Ho, J. S. *et al.* Wireless power transfer to deep-tissue microimplants. *Proc. Natl Acad. Sci. USA* **111**, 7974–7979 (2014).
- Laulicht, B., Traverso, G., Deshpande, V., Langer, R. & Karp, J. M. Simple battery armor to protect against gastrointestinal injury from accidental ingestion. *Proc. Natl Acad. Sci. USA* **111**, 16490–16495 (2014).
- Mercier, P. P., Lysaght, A. C., Bandyopadhyay, S., Chandrakasan, A. P. & Stankovic, K. M. Energy extraction from the biologic battery in the inner ear. *Nat. Biotechnol.* **30**, 1240–1243 (2012).
- Jung, W. *et al.* An ultra-low power fully integrated energy harvester based on self-oscillating switched-capacitor voltage doubler. *IEEE J. Solid-State Circuits* **49**, 2800–2811 (2014).
- El-Damak, D. & Chandrakasan, A. P. A 10 nW–1 μ W power management IC with integrated battery management and self-startup for energy harvesting applications. *IEEE J. Solid-State Circuits* **51**, 943–954 (2016).
- Zhang, S. *et al.* A pH-responsive supramolecular polymer gel as an enteric elastomer for use in gastric devices. *Nat. Mater.* **14**, 1065–1071 (2015).
- Yin, L. *et al.* Materials, designs, and operational characteristics for fully biodegradable primary batteries. *Adv. Mater.* **26**, 3879–3884 (2014).
- Lee, K. B. & Lin, L. Electrolyte-based on-demand and disposable microbattery. *IEEE J. Microelectromechanical Syst.* **12**, 840–847 (2003).
- Garay, E. F. & Bashirullah, R. Biofluid activated microbattery for disposable microsystems. *IEEE J. Microelectromechanical Syst.* **24**, 70–79 (2015).
- Kim, Y. J., Chun, S.-E., Whitacre, J. & Bettinger, C. J. Self-deployable current sources fabricated from edible materials. *J. Mater. Chem. B* **1**, 3781–3788 (2013).
- Hafezi, H. *et al.* An ingestible sensor for measuring medication adherence. *IEEE Trans. Biomed. Eng.* **62**, 99–109 (2015).
- Jimbo, H. & Miki, N. Gastric-fluid-utilizing micro battery for micro medical devices. *Sens. Actuat. B* **134**, 219–224 (2008).
- Mostafalu, P. & Sonkusale, S. Flexible and transparent gastric battery: energy harvesting from gastric acid for endoscopy application. *Biosens. Bioelectron.* **54**, 292–296 (2014).
- Di Maio, S. & Carrier, R. L. Gastrointestinal contents in fasted state and post-lipid ingestion: *in vivo* measurements and *in vitro* models for studying oral drug delivery. *J. Control. Release* **151**, 110–122 (2011).
- Roy, O. Z. & Wehnert, R. W. Improvements in biogalvanic energy sources. *Med. Biol. Eng.* **12**, 50–56 (1974).
- She, D., Tsang, M., Kim, J. K. & Allen, M. G. Immobilized electrolyte biodegradable batteries for implantable MEMS. In *18th Int. Conf. Solid-State Sensors, Actuators and Microsystems (TRANSDUCERS)* 494–497 (IEEE, 2015).
- Dietary Reference Intakes for Vitamin A, K, Arsenic, Boron, Chromium, Copper, Iodine, Iron, Manganese, Molybdenum, Nickel, Silicon, Vanadium, and Zinc* (Food and Nutrition Board, Institute of Medicine, USA, 2001).
- Haynes, W. M. *CRC Handbook of Chemistry and Physics* (CRC, 2015).
- Kear, G., Barker, B. D. & Walsh, F. C. Electrochemical corrosion of unalloyed copper in chloride media—a critical review. *Corros. Sci.* **46**, 109–135 (2004).
- Low Voltage Digitally Controlled Potentiometer, ISL23315* (Intersil, 2015).
- 8-Bit Flash Microcontroller with XLP Technology, PIC12LF1840T39A* (Microchip, 2014).
- Snoeck, V. *et al.* Gastrointestinal transit time of nondisintegrating radio-opaque pellets in suckling and recently weaned piglets. *J. Control. Release* **94**, 143–153 (2004).
- Hossain, M., Abramowitz, W., Watrous, B. J., Szpunar, G. J. & Ayres, J. W. Gastrointestinal transit of nondisintegrating, nonerodible oral dosage forms in pigs. *Pharm. Res.* **7**, 1163–1166 (1990).
- Traverso, G. *et al.* Microneedles for drug delivery via the gastrointestinal tract. *J. Pharm. Sci.* **104**, 362–367 (2015).
- Ultra Low Power Boost Converter with Battery Management for Energy Harvester Applications, BQ25504* (Texas Instruments, 2015).
- Santini, J. T. Jr, Cima, M. J. & Langer, R. A controlled-release microchip. *Nature* **397**, 335–338 (1999).
- Santini, J. T. Jr, Richards, A. C., Scheidt, R., Cima, M. J. & Langer, R. Microchips as controlled drug-delivery devices. *Angew. Chem. Int. Ed.* **39**, 2396–2407 (2000).

35. Singeap, A.-M. Capsule endoscopy: the road ahead. *World J. Gastroenterol.* **22**, 369 (2016).
36. Reardon, S. Electroceuticals spark interest. *Nature* **511**, 18 (2014).
37. Traverso, G. & Langer, R. Perspective: special delivery for the gut. *Nature* **519**, S19 (2015).
38. Niven, D. J. *et al.* Accuracy of peripheral thermometers for estimating temperature: a systematic review and meta-analysis. *Ann. Intern. Med.* **163**, 768–777 (2015).
39. Harpe, P., Gao, H., Dommele, R. V., Cantatore, E. & van Roermund, A. H. M. A 0.20 mm² 3 nW signal acquisition IC for miniature sensor nodes in 65 nm CMOS. *IEEE J. Solid-State Circuits* **51**, 240–248 (2016).
40. Yaul, F. M. & Chandrakasan, A. P. A 10 bit SAR ADC with data-dependent energy reduction using LSB-first successive approximation. *IEEE J. Solid-State Circuits* **49**, 2825–2834 (2014).
41. Paidimarri, A., Ickes, N. & Chandrakasan, A. P. A +10dBm 2.4GHz transmitter with sub-400pW leakage and 43.7% system efficiency. In *2015 IEEE Int. Solid-State Circuits Conf. (ISSCC) Digest of Technical Papers* 1–3 (IEEE, 2015).
42. Fojtik, M. *et al.* A millimeter-scale energy-autonomous sensor system with stacked battery and solar cells. *IEEE J. Solid-State Circuits* **48**, 801–813 (2013).
43. Kethu, S. R. *et al.* Endoluminal bariatric techniques. *Gastrointest. Endosc.* **76**, 1–7 (2012).
44. Rapoport, B. I., Kedzierski, J. T. & Sarpeshkar, R. A glucose fuel cell for implantable brain-machine interfaces. *PLoS ONE* **7**, e38436 (2012).
45. Schoellhammer, C. M. *et al.* Ultrasound-mediated gastrointestinal drug delivery. *Sci. Transl. Med.* **7**, 310ra168 (2015).
46. Nadeau, P. *et al.* Data for Prolonged energy harvesting for ingestible devices. *figshare* <http://dx.doi.org/10.6084/m9.figshare.4451420> (2017).

Acknowledgements

We thank J. Haupt, M. Jamiel and A. Hayward for help with the *in vivo* porcine work. We also thank A. Paidimarri for helpful discussions. A.P.C. was funded by Texas Instruments, the Semiconductor Research Corporation's Center of Excellence for Energy Efficient Electronics, and the Hong Kong Innovation and Technology Commission. R.L. was funded by a National Institutes of Health grant, EB-000244; a Max Planck Research Award, Ltr Dtd. 2/11/08; and the Alexander von Humboldt-Stiftung Foundation. G.T. was funded in part by the Division of Gastroenterology, Brigham and Women's Hospital.

Author contributions

P.N., D.E.-D., D.G., Y.L.K., N.R., R.L., A.P.C. and G.T. conceived and designed the research. P.N., D.E.-D., S.M., Y.L.K. and N.R. constructed the prototypes for testing. P.N., D.E.-D., D.G. and Y.L.K. conducted the *in vitro* characterization. P.N. wrote the software for the capsules and offline processing of the packets. P.N., D.E.-D., D.G., Y.L.K., C.C., L.B. and G.T. performed the *in vivo* pig experiments. P.N., D.E.-D., D.G., Y.L.K., N.R., R.L., A.P.C. and G.T. analysed the data and wrote the manuscript.

Additional information

Supplementary information is available for this paper.

Reprints and permissions information is available at www.nature.com/reprints.

Correspondence and requests for materials should be addressed to R.L., A.P.C. and G.T.

How to cite this article: Nadeau, P. *et al.* Prolonged energy harvesting for ingestible devices. *Nat. Biomed. Eng.* **1**, 0022 (2017).

Competing interests

The authors declare that provisional patent application no. 62/328,084, covering a portion of this work, was filed with the United States Patent and Trademark Office on 27 April 2016.